Study on the emitter infiltration of needle-capillary ionic liquid electrospray thruster

Cite as: AIP Advances **11**, 035234 (2021); https://doi.org/10.1063/5.0040081
Submitted: 10 December 2020 • Accepted: 14 February 2021 • Published Online: 19 March 2021

Senwen Xue, Li Duan and Qi Kang

Study on the emitter infiltration of needle-capillary ionic liquid electrospray thruster

Cite as: AIP Advances 11, 035234 (2021); doi: 10.1063/5.0040081
Submitted: 10 December 2020 • Accepted: 14 February 2021 •
Published Online: 19 March 2021

Senwen Xue, Li Duan, and Qi Kang[a]

AFFILIATIONS

Key Laboratory of Microgravity, Institute of Mechanics, Chinese Academy of Sciences, Beijing 100190, People's Republic of China and School of Engineering Sciences, University of Chinese Academy of Sciences, Beijing 100049, People's Republic of China

[a]Author to whom correspondence should be addressed: kq@imech.ac.cn

ABSTRACT

This article proposes a new emitter structure of needle-capillary ionic liquid electrospray thruster and carries out numerical simulation and theoretical analysis to discover the emitter infiltration effect under the conditions of no liquid supply and liquid supply. Emitter physical dimensions L, d, θ, β and the contact angles α, γ between the ionic fluid and the structure jointly determine the configuration of the meniscus. By analyzing the influence of various variables on the infiltration, a complete emitter infiltration law of needle-capillary ionic liquid electrospray thruster is summarized. In addition, the phenomena of infiltration relaxation and periodical infiltration oscillation are found in the numerical simulation under the condition of liquid supply, which provide an important basis for the optimization of the emitter structure. Considering Bond number $\ll 10^{-2}$ and working in a space environment, the liquid is mainly affected by surface tension and viscous force. Meanwhile, the meniscus formed by the ionic fluid satisfies the requirement that it has rotational axis symmetry and constant mean curvature surface, thereby obtaining the mathematical analytical expression of the quasi-static meniscus, the Delaunay surface. The numerical simulation results and analytical solutions are fitted, and an excellent consistency is obtained with an extremely small fitting deviation. Besides, the classification inferences of the type of Delaunay surface to which the meniscus belongs to are explored.

I. INTRODUCTION

Micro-electric propulsion technology occupies an important position in space missions such as the orbit maintenance of micro/nano-satellites (mass < 100 kg), attitude control, and satellite formation flying.[1] As a reliable solution, the ILET (Ionic Liquid Electrospray Thruster) has demonstrated its advantages of small size, light weight, high specific impulse, continuously adjustable thrust, high thrust accuracy, and no need for neutralization. Compared with other micro-thrusters such as the PPT (Pulsed Plasma Thruster), VAT (Vacuum Arc Thruster), and FEEP (Field Emission Electric Propulsion Thruster), the ILET has great potential to be a main propulsion device for space gravitational wave detection satellites. The American Busek company has developed a CMNT (Colloid Micro-Newton Thruster) for ST7-DRS (Space Technology 7 Disturbance Reduction System) and LISA (Laser Interferometer Space Antenna) missions. These drag-free missions required precision micro-thrusters to provide a low-noise spacecraft position controlled within ~10 nm of free-floating masses, used to detect gravitational waves. Both missions have similar micro-thruster performance requirements: a thrust range of 5 μN–30 μN, a thrust resolution < 0.1 μN, and thrust noise < 0.1 μN Hz$^{-1/2}$ over the ST7-DRS and LISA measurement bandwidths.[2–4] The CMNT was successfully ignited in orbit in January 2016. Eight thrusters were in stable working condition with the thrust range of 5 μN–30 μN and thrust resolution < 0.1 μN, which met the requirements for drag-free control in the LISA mission.[5]

According to the difference in the ILET emitter structure, it can be classified into external infiltration type, capillary type, and porous media type. The external infiltration type achieves complete infiltration with the ionic liquid by changing the structure and material of the emitter and forms a liquid film on the external of the

emitter to achieve the purpose of continuously infiltrating the emitter to ensure continuous emission. The SPL (Space Propulsion Laboratory) of MIT in the United States has developed a two-dimensional array ILET using MEMS (Micro-Electro-Mechanical System) technology, which can achieve the complete external infiltration of the emitter. The integrated density of the emitter is 502/113 mm^2, the specific impulse is 3000 s, the thrust is 13 μN, the thrust density is 0.15 N/m^2, the power is 275 mW, and the efficiency is 85%.[6] The capillary type requires a liquid supply system composed of a micropump, a micro-valve, a micro-flow channel, a pipeline, and a liquid storage device for initiative supply. The piezo-actuated microvalve liquid supply system developed by the BUSEK company and JPL (Jet Propulsion Laboratory) can achieve thrust control with a resolution less than 0.1 μN, and the response time is less than 0.5 s.[7] The porous media type passively supplies the propellant with the liquid capillary force through the material pores. The American ACCION company and MIT have developed a series of ILETs using porous tungsten,[8] porous nickel,[9] and porous glass[10] as emitter materials. The size of a single module is 1.44 × 1.44 × 1.41 cm^3, the mass is 1.8 g, the power is 0.15 W, the maximum thrust is 12.5 μN, and the specific impulse is 1150 s.[11] These three liquid supply modes all encounter the tough problem of emitter infiltration. The infiltration effect has a great influence on the emission mode of the thruster, the consistency and stability of thrust, and the thrust noise. Therefore, studying the liquid spreading pattern on the emitter external, liquid surface configuration, infiltration, and infiltrating velocity is particularly important for improving the performance of the ILET.

In response to the problem that the traditional ILET cannot continuously infiltrate the tip of the emitter, UCLA has proposed a new hybrid emitter structure that consists of a capillary emitter with a protruding and coaxial needle. Due to the different infiltrating effects, two emission modes, externally wetted and capillary modes, were found in the experiment. A needle in the center of a capillary emitter promotes stable emission with high specific impulse at low flow rate in an externally wetted mode. When the flow rate is increased, the meniscus extends past the needle to emit with high thrust-to-power in a capillary or cone-jet mode. Variable mode emission has been achieved through controlling the meniscus configuration to infiltrate the needle or the capillary. Dual-mode propulsion describes the use of a propulsion system operating on a single propellant supply to offer both high specific impulse and high thrust operating modes.[12]

This paper proposes a needle-capillary model that is more conducive to the emitter infiltration and explores the infiltration performance of the ionic liquid when no electric field is applied. Through the method of numerical simulation, the liquid spreading pattern, liquid surface configuration, and infiltrating velocity of the ionic liquid on the external of the needle-capillary emitter are observed. We discuss the transform of the ILET emission mode caused by infiltration and the varying thruster property under different emission modes, which provides guidance for thruster design, experiment, and optimization.

II. PHYSICAL MODEL OF NEEDLE-CAPILLARY EMITTER

In general, the ILET consists of an emitter and extractor. A strong electric field is formed between the emitter and the extractor. The emitter is infiltrated by the ionic liquid composed of a pure anion and pure cation, and a Taylor cone appears at the maximum electric field intensity. At the tip of the Taylor cone, if the electric field energy is large enough, ions, ion clusters, or charged droplets will break through the liquid energy barrier and form a stable cone jet at the emitter. The composition of the cone jet is very complex. If the emission component is a charged droplet, the ILET is in the droplet emission mode that has high thrust but exceedingly low specific impulse. If the emission component is a pure ion or pure ion cluster, the ILET is in the pure ion emission mode that has low thrust but high specific impulse. The emission mode is closely related to the infiltrating effect of the emitter, which determines the way in which the ionic liquid breaks through the energy barrier, thus affecting the performance of the thruster.

The emitter of the needle-capillary ILET is a rotationally symmetrical structure, and a two-dimensional 1/2 model is selected for physical modeling. The structure dimensions and boundary conditions are shown in Fig. 1. Compared with the needle emitter, due to the existence of the E_iD (i = 1, 2, 3, 4) edge, the needle-capillary emitter has a flow controllable ionic liquid supply to infiltrate the tip. This model combines the advantages of the needle emitter with a small tip size, which makes it easy to launch, and the capillary emitter with the controllable flow so that it is difficult to pollute the emitter array, so as to realize the transportation and management of the ionic fluid. L is the height of the needle exposed to the capillary, θ is the half angle of the needle, d_i (i = 1, 2, 3, 4) is the shortest distance from the needle to the capillary, β is the inclination angle of the capillary (it is stipulated that when the cylinder wall is vertical,

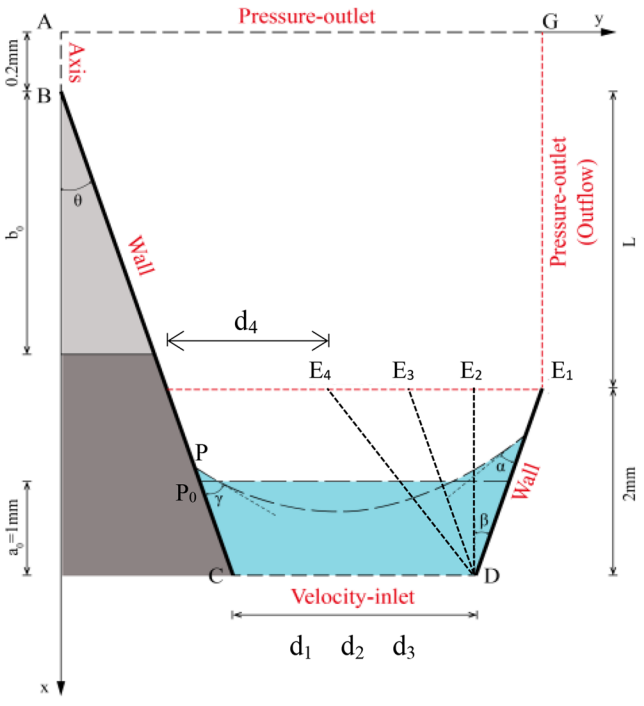

FIG. 1. Two-dimensional 1/2 physical model graph of the needle-capillary emitter.

TABLE I. Propellant properties (25 °C, 1 atm).

Abbreviation	μ (Pa s)	σ (N/m)	ρ (kg/m^3)
EMI-TFSI	0.034	0.0364	1520

$\beta = 0^\circ$ and β is positive when the E_iD edge rotates clockwise), γ is the needle-liquid contact angle, and α is the capillary-liquid contact angle. When $\beta > 0$, the capillary is at E_1D, corresponding to d_1. When $\beta = 0$, the capillary is at E_2D, corresponding to d_2. When $-\beta = \theta > 0$, the capillary is at E_3D, corresponding to d_3. When $\beta < 0$, the capillary is at E_4D, corresponding to d_4. These variables collectively affect the meniscus configuration and the emitter infiltration.

EMI-TFSI {1-ethyl-3-methylimidazolium bis[(trifluoromethyl) sulfonyl]imide} is selected as the numerical simulation working medium in this paper, and the physical properties are shown in Table I. Ionic liquids are molten salts composed of pure ions at 25 °C with extremely low saturated vapor pressure, extremely high conductivity, reliable thermostability, and chemical stability.

III. ANALYTICAL FITTING AND NUMERICAL SIMULATION

A. Analytical expression of infiltration surface

The meniscus properties originated from the Young–Laplace equation, which is expressed as follows:[13]

$$\frac{y''}{\left(1+y'^2\right)^{3/2}} - \frac{1}{y\sqrt{1+y'^2}} = -\frac{\Delta p}{\gamma^*} = H, \tag{1}$$

where Δp is the pressure difference between the inside (liquid) and the outside (air) of the meniscus, γ^* is the surface tension, and $x \to y(x)$ is the curve path of meridian of the meniscus. In the case $H \neq 0$, the integration of the Young–Laplace equation leads to a first integral

$$\lambda = \frac{y}{\sqrt{1+y'^2}} + \frac{Hy^2}{2}, \tag{2}$$

where λ is a constant at all points of the profile. Then, Eq. (2) may be rewritten as follows:

$$1 + y'^2 = \frac{4y^2}{H^2\left(y^2 - \frac{2\lambda}{H}\right)^2}. \tag{3}$$

Depending on the sign of H and λ, Eq. (3) can be expressed as follows:

$$1 + y'^2 = \frac{4a^2y^2}{\left(y^2 + \varepsilon b^2\right)^2}, \tag{4}$$

where $a = \frac{1}{|H|}$, $b^2 = \left|\frac{2\lambda}{H}\right|$, with $\varepsilon = \pm 1$. Equation (4) recalls Delaunay's roulettes that describe the surface of revolution with a constant mean curvature. When $\varepsilon = 1$, the meridional profile is a portion of unduloid, where $\varepsilon = -1$ corresponds to a portion of nodoid. The meniscus formed by the ionic liquid and the structures meets the assumptions of axisymmetric rotation and constant mean curvature surface. Therefore, the infiltration surface belongs to a part of the Delaunay surface.

According to the given geometrical data of the meniscus (L, d, θ, γ, β, α), the variables L, d, θ, and γ are usually fixed in an ILET; the shape of the meniscus is only associated with α and β. In this section, the classification inference of the type of Delaunay surface to which the meniscus belongs to is established. Analyses will be limited here to nodoid and unduloid shapes.[14,15]

Result 1. If the structure of the ILET is such that

$$\alpha + \beta > 90^\circ, \tag{5}$$

then the meridional profile of the meniscus may be a portion of unduloid; the profile curve of an unduloid has a parameterization of the following type:[16]

$$x(t) = \frac{b^2}{a}\int_0^t \frac{1}{(1+e_1\cos u)\sqrt{1-e_1^2\cos^2 u}}\,\mathrm{d}u,$$
$$y(t) = b\sqrt{\frac{1-e_1\cos t}{1+e_1\cos t}}, \tag{6}$$

where a and b, with $|a| > |b|$, represent the semi-major and semi-minor of an ellipse, respectively, and the focus and eccentricity of the ellipse are ε_1 and e_1. Moreover, ε_1 and e_1 are given by the following equations:

$$\varepsilon_1 = \sqrt{a^2 - b^2},$$
$$e_1 = \frac{\varepsilon_1}{a}.$$

Result 2. If the structure of the ILET is such that

$$\alpha + \beta \leq 90^\circ, \tag{7}$$

then the meridional profile of the meniscus may be a portion of nodoid; the profile curve of a nodoid has a parameterization of the following type:[16]

$$x(t) = \frac{b^2}{a}\int_0^t \frac{\cos u}{(e_2+\cos u)\sqrt{e_2^2-\cos^2 u}}\,\mathrm{d}u,$$
$$y(t) = b\sqrt{\frac{e_2-\cos t}{e_2+\cos t}}, \tag{8}$$

where a and b with $a > 0$, $b > 0$, ε_2 and e_2 are given by the following equations:

$$\varepsilon_2 = \sqrt{a^2 + b^2},$$
$$e_2 = \frac{\varepsilon_2}{a}.$$

B. Numerical simulation results without propellant supply

The variables L, d, θ, β, α, and γ affect the emitter infiltration collectively. As a result, it is particularly significant that the emitter infiltration law under the influence of a single variable should be studied. In order to facilitate comparison, the emitter infiltration results are analyzed by the dimensionless method. The proportion

of infiltration part $h/(L + 2)$ is a dimensionless quantity that is used to characterize the infiltration degree, and h is the vertical distance from the leading edge of the liquid climbing on the needle side to the bottom of the needle.

1. Capillary inclination β

As shown in Fig. 2, when L = 3 mm, θ = 10°, d = 1 mm, and γ = 0°, the effects of variables α and β on emitter infiltration are investigated. The five pairs of fitting curves in Fig. 2(a2) correspond to five points (black circles) in Fig. 2(a1), and the emitter model corresponding to each point has a unique meniscus. As shown in Fig. 2(a1), when α is constant and β is increased, the proportion of infiltration part shows a parabolic upward trend. Concurrently, when β is constant and α is increased, the proportion of infiltration part increases. It illustrates that the infiltration can be improved by increasing α or β.

α indicates the contact angle between the capillary (E_iD edge) and the ionic liquid. β determines the position of the capillary. Both α and β are variables related to the capillary. According to the inference in Sec. III A and as shown in Fig. 2(a2), the value of α + β will affect the classification of the Delaunay surfaces to which the meniscus belongs, thus forming different liquid surface configurations. As shown in the blue part of Fig. 2(a2), the classification and configuration of the meniscus collectively determine the proportion of infiltration part and liquid reserves. In Fig. 2(a2), only the meniscus with α = 85° and β = 50° belongs to an unduloid and others belong to a nodoid. Although the height of the capillary is kept at 2 mm, the influence of the capillary height on infiltration can be reflected by the study of the variable L.

2. Needle half angle θ

As shown in Fig. 3, when L = 3 mm, d = 1 mm, and γ = 0°, the effects of variables α and θ on emitter infiltration are investigated. The value of α is between 0° and 85°, and the value of α + β determines the classification of the Delaunay surface to which the meniscus belongs. It is necessary to investigate the influence of variables α and θ on emitter infiltration under different β. Therefore, β = 30°, β = 0°, and β = −30° are selected for (a)–(c), respectively. The six pairs of fitting curves in Figs. 3(a2), 3(b2), and 3(c2) correspond to six points (black circles) in Figs. 3(a1), 3(b1), and 3(c1), respectively. The six points include two cases of α = 0° and α = 85° to ensure that the requirements of α + β ≤ 90° or α + β > 90° are satisfied.

θ is the half angle of the needle, which has a great impact on the emission performance of the ILET, mainly reflected in the initial emission voltage and emission mode. The trend of the curve is shown in Figs. 3(a1), 3(b1), and 3(c1); there exists an optimal θ, which makes emitter infiltration the most outstanding. The optimal θ for different curves is approximately between 15° and 35°. Similarly, when β is constant and α is increased, the proportion of infiltration part increases. Observing the curve corresponding to the same α in Figs. 3(a1), 3(b1), and 3(c1), when α is constant and β is increased, the amplitude of the curve will move up as a whole, which means that the proportion of infiltration part increases. This conclusion is consistent with the curve changing rule shown in Fig. 2. In Figs. 3(a2), 3(b2), and 3(c2), only the meniscus of Fig. 3(a2) with α = 85° and β = 50° belongs to an unduloid and others belong to a nodoid.

3. Needle height L

As shown in Fig. 4, when θ = 10°, d = 1 mm, and γ = 0°, the effects of variables α and L on emitter infiltration are investigated. The influence of α + β value on the classification of the Delaunay surface to which the meniscus belongs is also considered. Hence, β = −30°, β = 0°, and β = 30° are selected in Figs. 4(a), 4(c), and 4(d), respectively, and β = −10° in Fig. 4(b) makes the needle (BC edge) and the capillary (E_iD edge) parallel. This parallel structure weakens the influence of α on emitter infiltration, which shows that the distribution of curve clusters composed of different α in Fig. 4(b1) is more compact. The six pairs of fitting curves in Figs. 4(a2), 4(b2), 4(c2), and 4(d2) correspond to six points (black circles) in Figs. 4(a1), 4(b1), 4(c1), and 4(d1), and all of the six pairs of fitting curves have minimal fitting errors. As shown in Figs. 4(a1), 4(b1), 4(c1), and 4(d1), when α is constant, the proportion of infiltration part decreases linearly with the increasing L. Meanwhile, when β is constant, the proportion of infiltration part increases with the increasing α. Observing the curve corresponding to the same α in

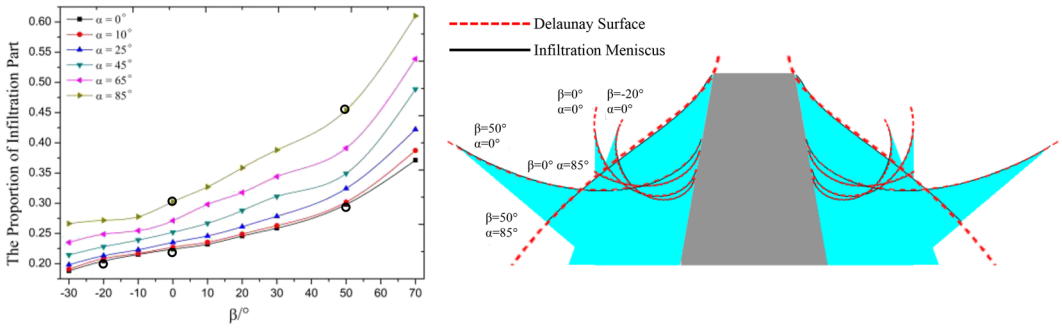

(a1) (a2)

FIG. 2. L = 3 mm, θ = 10°, d = 1 mm, γ = 0°, the effect of β and α on static infiltration. (a1) Numerical simulation trends. (a2) Fit of theoretical and numerical results.

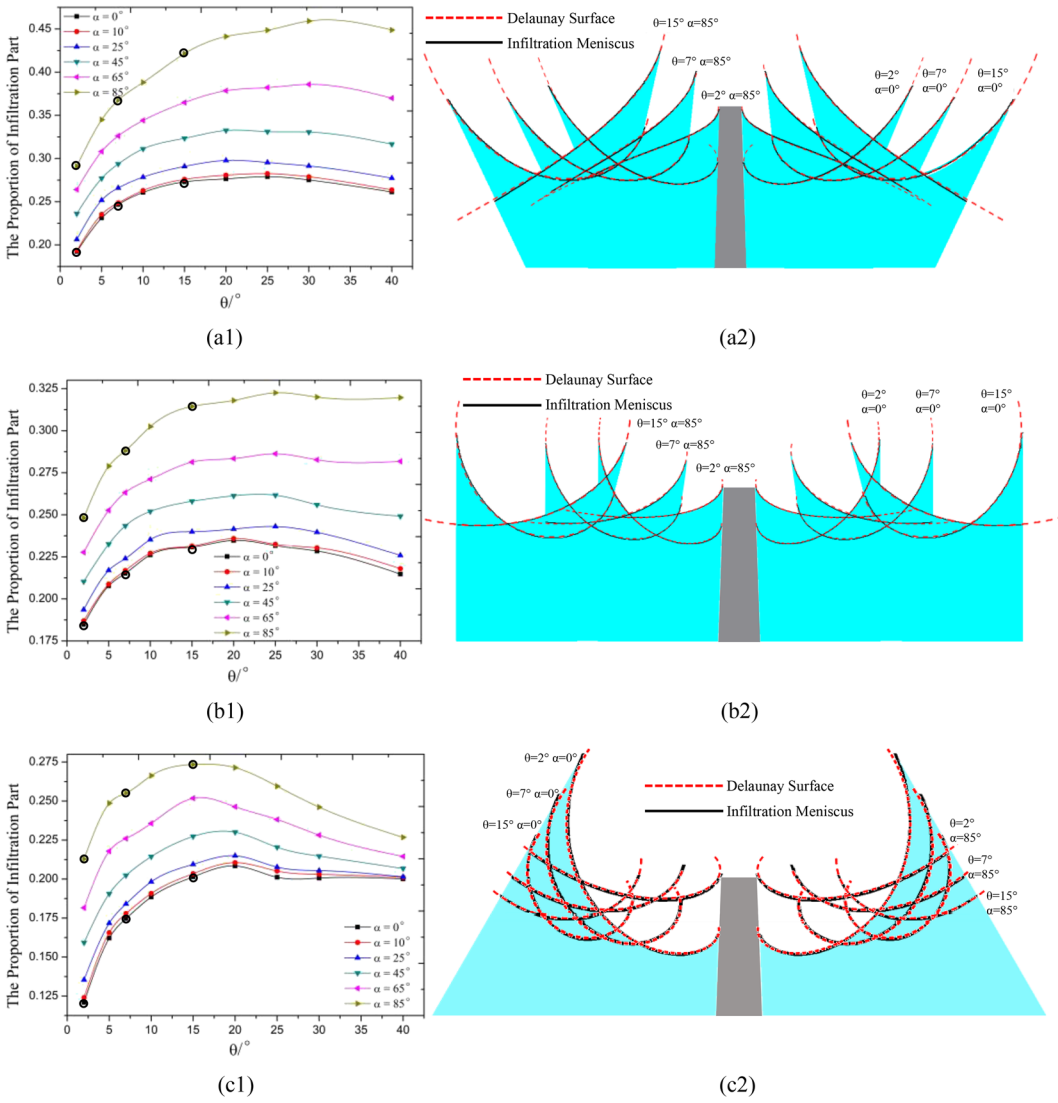

FIG. 3. L = 3 mm, d = 1 mm, γ = 0°, the effect of θ and α on static infiltration. (a) β = 30°, (b) β = 0°, (c) β = −30°. (a1), (b1), and (c1) Numerical simulation trends. (a2), (b2), and (c2) Fit of theoretical and numerical results.

Figs. 4(a1), 4(b1), 4(c1), and 4(d1), when α is constant and β is increased, the amplitude of the curve will move up as a whole, which means that the proportion of infiltration part increases. This conclusion is consistent with the curve changing rule shown in Fig. 2 as well.

L is the height of the needle exposed to the capillary. Although the shorter L is able to obtain a larger proportion of infiltration part and better mechanical stability, there is a great possibility that the emitter will be wrapped by the ionic liquid, which eventually leads to needle failure and enters the pure charged droplet emission mode dominated by the capillary. It is difficult for higher L to form an ionic liquid film to completely infiltrate the emitter, even if the meniscus formed by the ionic liquid is driven by a strong electric field. It will be seen that the shortest L should be selected based on the premise that the emitter can be completely infiltrated and pure ion emission can be achieved. In Figs. 4(a2), 4(b2), 4(c2), and 4(d2), only the meniscus of Fig. 4(d2) with α = 85° and β = 50° belongs to an unduloid and others belong to a nodoid.

4. Distance from needle to capillary d_i

As shown in Fig. 5, when θ = 10°, d = 3 mm, and γ = 0°, the effects of variables α and d on emitter infiltration are investigated. Likewise, β = −30°, β = −10°, β = 0°, and β = 30° are selected for (a)–(d), respectively. The six pairs of fitting curves in Figs. 5(a2), 5(b2), 5(c2), and 5(d2) correspond to six points (black

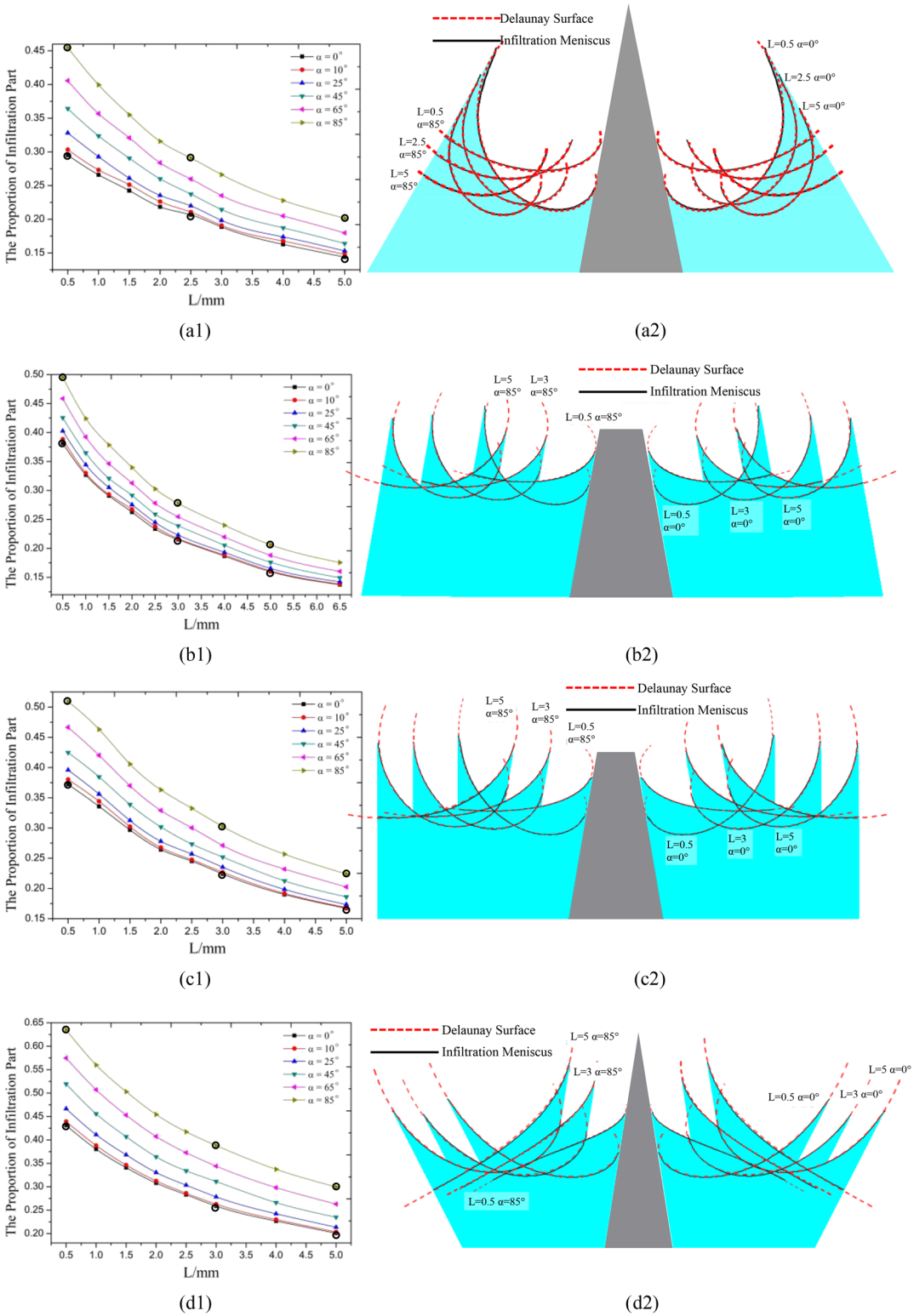

FIG. 4. θ = 10°, d = 1 mm, γ = 0°, the effect of L and α on static infiltration. (a) β = −30°, (b) β = −10°, (c) β = 0°, (d) β = 30°. (a1), (b1), (c1), and (d1) Numerical simulation trends. (a2), (b2), (c2), and (d2) Fit of theoretical and numerical results.

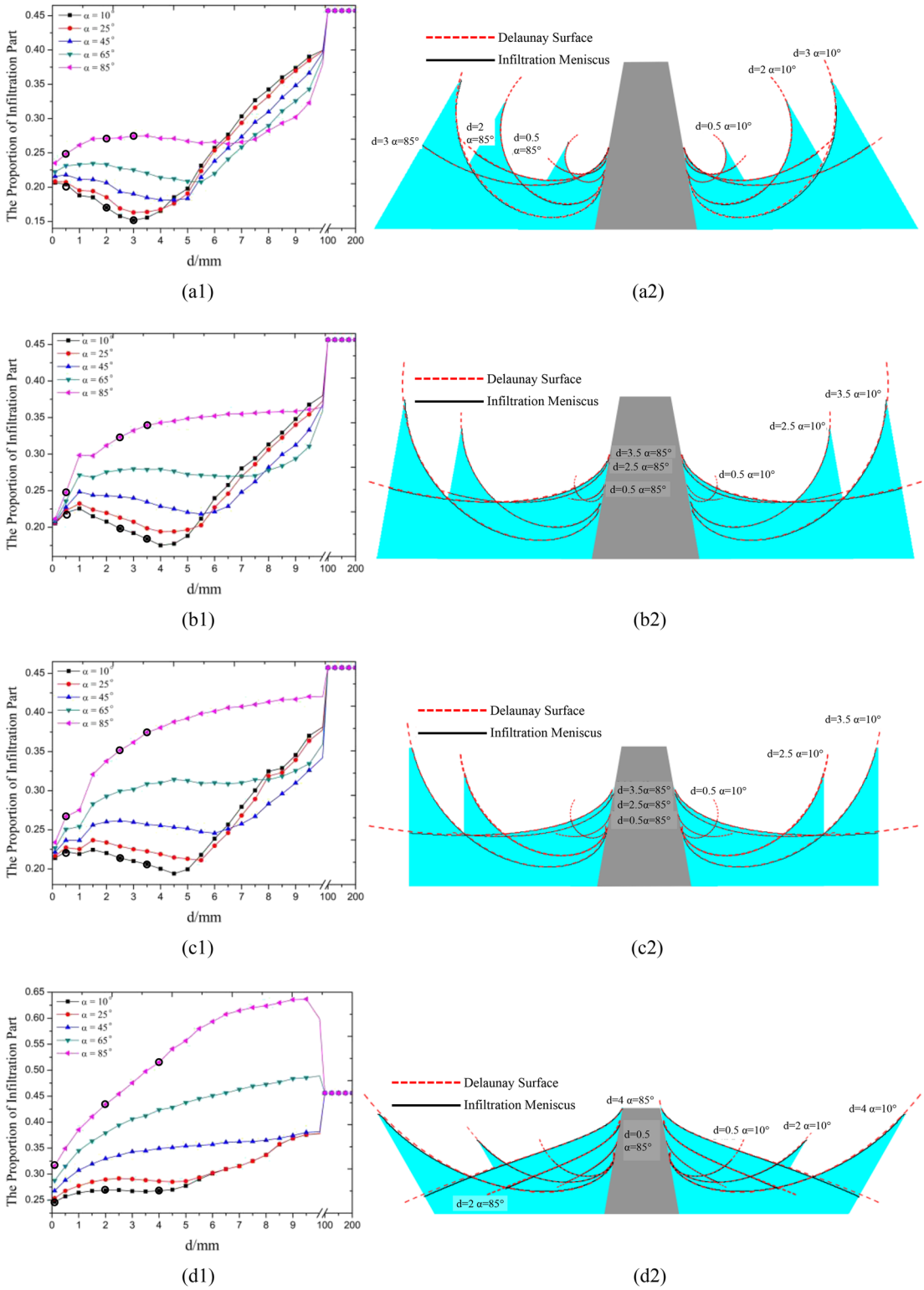

FIG. 5. θ = 10°, L = 3 mm, γ = 5°, the effect of d and α on static infiltration. (a) β = −30°, (b) β = −10°, (c) β = 0°, (d) β = 30°. (a1), (b1), (c1), and (d1) Numerical simulation trends. (a2), (b2), (c2), and (d2) Fit of theoretical and numerical results.

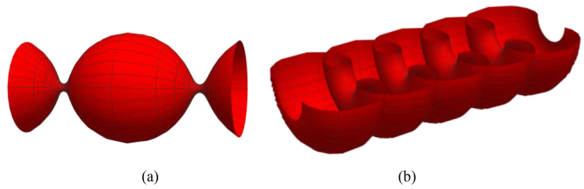

FIG. 6. Three-dimensional graph of two Delaunay surfaces. (a) Unduloid $a = 2$, $b = 1$; (b) 1/2 profile of the nodoid $a = 0.8$, $b = 1$.

circles) in Figs. 5(a1), 5(b1), 5(c1), and 5(d1), respectively. The variable d increases continuously in the range of 0.1 mm–10 mm. The curves corresponding to different α in Figs. 5(a1), 5(b1), and 5(c1) show strong nonlinearity. The difference is that the curves corresponding to different α in Fig. 5(d1) show a linear upward trend. In striking contrast to the variables L, β, and θ, the infiltration curves of the identical β and diverse α no longer have similar curvatures due to the variation of the proportion of infiltration part caused by the variable d. When d is a smaller value and β is constant, the proportion of infiltration part increases with the increasing α. Beyond these ranges, it is impossible to increase the proportion of infiltration part by simply increasing α. At last but not the least, observing the curve corresponds to the same α in Figs. 5(a1), 5(b1), 5(c1), and 5(d1); when α is constant and β is increased, the amplitude of the curve will move up as a whole, which means that the proportion of infiltration part increases. This conclusion is always consistent with the curve changing rule shown in Fig. 2.

d_i (i = 1, 2, 3, 4) is the shortest distance from the needle to the capillary. From the above analysis, it can be seen that simply changing d is not able to achieve the purpose of increasing the proportion of infiltration part, which should be analyzed according to the specific value of α and β. It will lead to capillary losing efficacy if d is too large. No matter how the α and β change, it will not affect the emitter infiltration. Furthermore, the capillary will be deprived of the function of transporting and managing ionic liquids. In addition, the variable d directly determines the liquid reserves of the emitter. In particular, the blue part corresponding to the six pairs of fitting curves in Figs. 5(a2), 5(b2), 5(c2), and 5(d2) represents the volume of the ionic liquid. The larger the area of the blue part, the more the liquid reserves of the emitter. The maximum proportion of infiltration part ought to be detected under the premise of guaranteeing the fewest liquid reserves, which is beneficial to the stability of thrust and specific impulse. At the same time, it is explored that, in Figs. 5(a2), 5(b2), 5(c2), and 5(d2), only the meniscus of Fig. 5(d2) with $\alpha = 85°$ and $\beta = 50°$ belongs to an unduloid and others belong to a nodoid.

It can be seen from Fig. 6 that the Delaunay surface is a three-dimensional periodic rotational axisymmetric surface, and its profile is a two-dimensional periodic axisymmetric curve. The meniscus formed by the infiltration surface conforms to the assumption of constant mean curvature surface. Besides, the meniscus is a free surface without any external force. To sum up, the meniscus is a part of the Delaunay surface. As shown in Fig. 7, a complete period of nodoid and unduloid was selected, and the curves within a whole period were divided. It can be found that the nodoid curve in a complete period is composed of A_1B_1, B_1C_1, and C_1D_1. Unlike nodoid, the unduloid curve in a complete period is composed of A_2B_2, B_2C_2, and C_2D_2. When the meniscus satisfies the inference of result 1 in Sec. III A, the meniscus is either a part of B_2C_2 in the unduloid curve or a part of A_1B_1 in the nodoid curve. When the meniscus satisfies the inference of result 2 in Sec. III A, the meniscus must be a part of A_1B_1 in the nodoid curve definitely. By fitting different menisci with the Delaunay surfaces, excellent consistencies and extremely

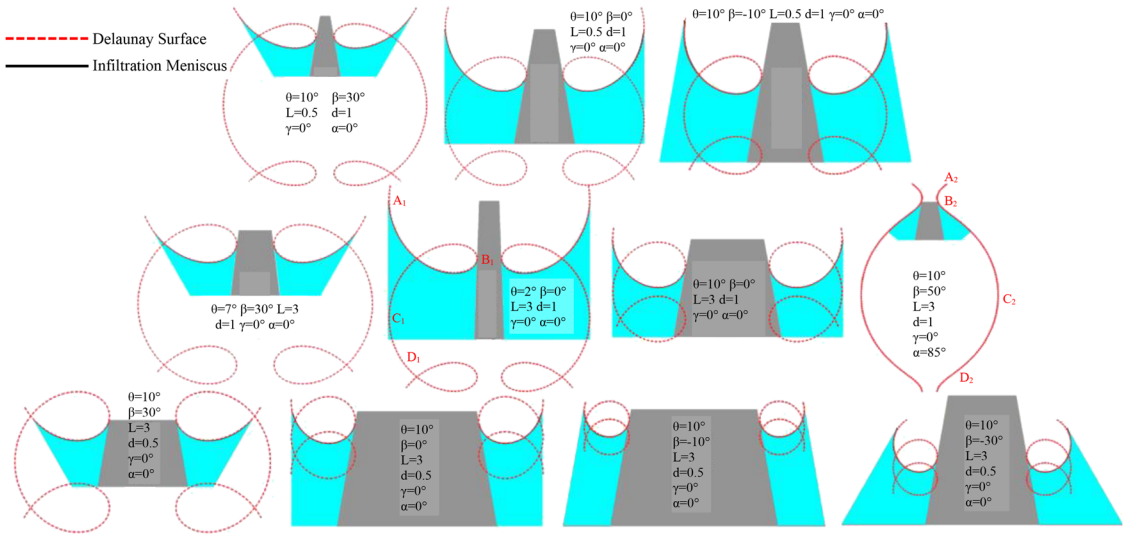

FIG. 7. Graph of fitting two kinds of Delaunay surfaces with different menisci.

small fitting deviations are obtained. The research studies indicate that the variables L, d, θ, β, and α have significant effects on emitter infiltration.

C. Numerical simulation results with propellant supply

According to Sec. III B, it has been affirmed that the quasi-static meniscus is a part of the Delaunay surface. As a result, in order to highlight the influence of variables L, d, θ, β, and α on the emitter infiltrating velocity and P_{max} that is the limit position of the liquid climbing leading edge on the needle side, it is necessary to keep the meniscus close to the quasi-static state as far as possible during the liquid supply. Excessive liquid feeding speed will lead to the meniscus not close to the quasi-static state and cover up the influence of variables L, d, θ, β, and α on the emitter infiltrating velocity. Meanwhile, too small liquid feeding speed will multiply the calculation cost. Consequently, it is significant to give the boundary condition of the CD edge (velocity-inlet) in Fig. 1 an appropriate liquid feeding speed. Based on the above analysis, the liquid feeding speed should be at least less than the average velocity of the liquid climbing leading edge on the needle side when the liquid level transforms from a_0 in Fig. 1 to the quasi-static meniscus. In order to explore the average velocity of the liquid climbing leading edge on the needle side, all models in Sec. III B without liquid supply are sampled. There are 96 sampling points covering the extremum of all variables. The sampling results are shown in Fig. 8, which demonstrate the average velocity distribution is in the order of 1×10^{-1}–1×10^{1}. In summary, it is reasonable that the liquid feeding speed is less than 1×10^{-1}. Ultimately, the liquid feeding speed was determined to be 0.01 mm/s.

In the case of no liquid supply, the influence of variables L, d, θ, β, and α on emitter infiltration is studied. The quasi-static configuration of the meniscus and the inference that the type of Delaunay surface to which the meniscus belongs are analyzed. As shown in Fig. 1, the height of the initial liquid level a_0 = 1 mm, and the boundary condition of the CD edge (velocity-inlet) is set to 0, which

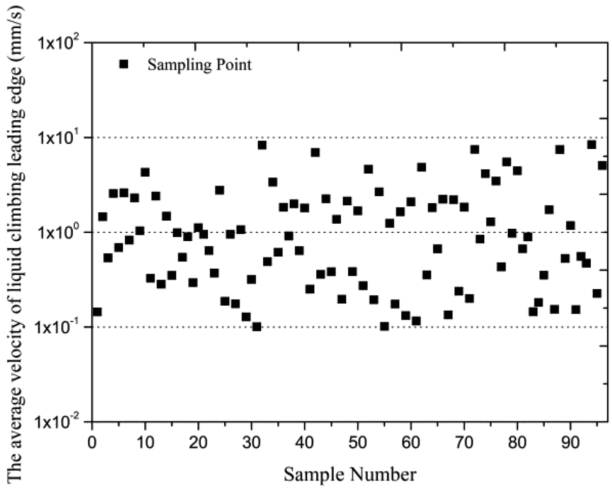

FIG. 8. Average velocity distribution of the liquid climbing leading edge on the needle side.

makes the volume of the liquid fixed. Therefore, when the initial liquid level transforms from P_0 to P on the quasi-static meniscus, the limit position P_{max} (the maximum proportion of infiltration part) that the liquid leading edge on the needle side can climb to has not been observed. So to acquire the position of P_{max} and the infiltrating response time t_{min} (the shortest time required to reach the maximum proportion of infiltration part), as well as the law of emitter infiltrating velocity with respect to the variables L, d, θ, β, and α, it is momentous to discuss the case of liquid supply. Hence, if the boundary condition of the CD edge (velocity-inlet) is set to 0.01 mm/s, the liquid volume will continue to increase until the overflow occurs at point E_i. At this moment, in addition to P_{max} and t_{min}, the spreading pattern of ionic liquids on the needle external and the law of emitter infiltrating velocity with regard to variables L, d, θ, β, and α can be surveyed. In view of this, the research on the liquid supply conditions has great guiding significance for the infiltration optimization of the needle-capillary ILET.

1. Capillary inclination β

As shown in Fig. 9, when L = 3 mm, θ = 20.83°, d = 1 mm, and γ = 1°, the effects of variables α and β on the emitter infiltrating velocity are investigated. For the sake of exploring the infiltrating pattern of the nodoid and unduloid under the influence of variables α and β, it is essential to consider the emitter model that satisfies the requirement of $\alpha + \beta \le 90^\circ$ or $\alpha + \beta > 90^\circ$; thus, two contact angles α = 5° [Fig. 9(a1)] and α = 85° [Fig. 9(a2)] should be set. In particular, this paper discusses the emitter model with θ = 20.83° and β = −20.83° so that the needle (BC edge) is parallel to the capillary (E_iD edge).

As shown in Fig. 9, the emitter infiltrating velocity corresponding to different β remains constant. The emitter infiltrating velocity decreases and the emitter infiltrating response time t_{min} increases with the increasing β gradually. Besides, enlarging α or β can elevate the position of P_{max}, which increases the proportion of infiltration part. This conclusion is consistent with the infiltration law obtained in Sec. III B 1. Comparing the infiltration curves with the same β in Figs. 9(a1) and 9(a2), it is found that α has minimal impact on the infiltrating velocity. When the ionic liquid overflows at the E_i point on the capillary side, the leading edge of the liquid climbing on the needle side reaches P_{max}. In the meantime, either the average infiltrating velocity on the needle side is 0 or the absolute infiltrating velocity is 0. The average infiltrating velocity is 0, which signifies that the location of P_{max} changes periodically (zone III). Similarly, the absolute infiltrating velocity is 0, which signifies the location of P_{max} is fixed (zone II).

As shown in zone I of Fig. 9(a1) (α = 5°), the infiltration relaxation is designated as a phenomenon that the proportion of infiltration part increases first and then decreases at the leading edge of the liquid climbing on the needle side. In contrast to α = 5°, the phenomenon of infiltration relaxation does not exist in Fig. 9(a2) (α = 85°). The infiltration relaxation is merely related to the variable α that started from the premise that an appropriate d guarantees the realization of capillary function. Furthermore, the smaller the α is, the more likely the infiltration relaxation will exist. On the premise that the infiltration relaxation has already occurred, the smaller the β is, the more obvious the infiltration relaxation is, which manifests that the proportion of infiltration part increases more first and then decreases more. The reason for infiltration relaxation may be

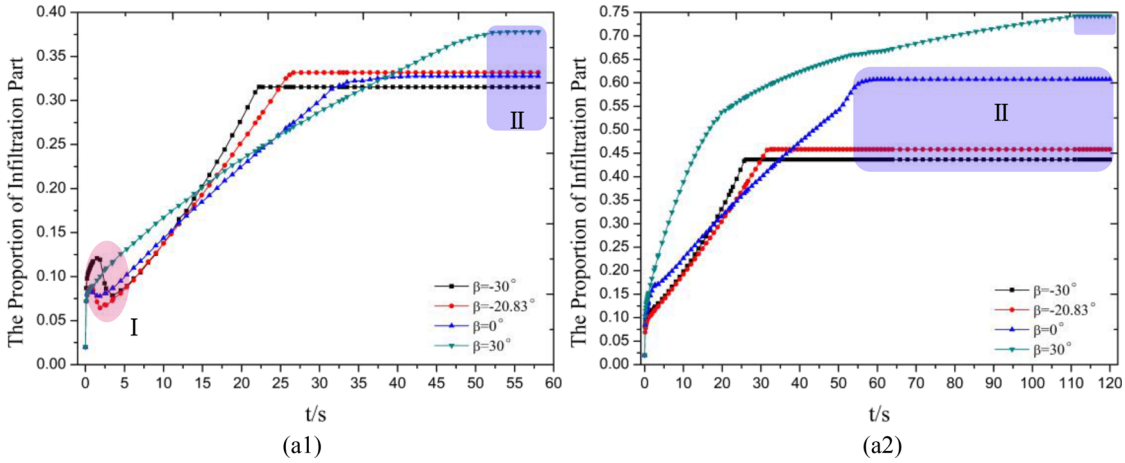

FIG. 9. θ = 20.83°, L = 3 mm, d = 1 mm, γ = 1°, the effect of β and α on dynamic infiltration. (a1) α = 5°; (a2) α = 85°.

caused by the residual acceleration that originates from the interaction of liquid viscous force and inertial force when the initial liquid level suddenly enters the numerical calculation environment of g = 0 m/s^2. As shown in Fig. 16, in the process of the residual acceleration changing to 0 (t = 0.098 s to t = 1.862 s), there exists a unique situation for the model with smaller α that more liquids tend to climb along the capillary (E_iD edge) preferentially and then climb along the needle (BC edge), which eventually leads to the infiltration relaxation. The ionic liquid will suddenly enter the internal of the emitter through the CD edge when the ILET is working in space. It signifies that the initial liquid level suddenly is exposed to the environment of g = 0 m/s^2. Based on the analysis of reality, the initial conditions set in the numerical calculation are reasonable and the phenomenon of infiltration relaxation also exists objectively during the emitting of the ILET.

2. Needle half angle θ

As shown in Fig. 10, when L = 3 mm, d = 1 mm, and γ = 1°, the effects of variables α and θ on the emitter infiltrating velocity are investigated. The classification discussion is arranged in this way so that in Figs. 10(a1), 10(b1), and 10(c1) α = 5°, Figs. 10(a2), 10(b2), and 10(c2) α = 85°, where (a) β = −30°, (b) β = 0°, (c) β = 30°. It ensures that the infiltration patterns of nodoid (α + β ≤ 90°) and unduloid (α + β > 90°) under the influence of variables can be examined.

As shown in Figs. 10(a1) θ = 15°, θ = 20° and 10(a2) θ = 2°, θ = 15°, θ = 20°, the slopes of curves increase gradually before the curves reach an inflection point. As shown in Figs. 10(a1) θ = 2°, θ = 35°, 10(a2) θ = 35° and 10(b), the slopes of curves keep constant before the curves reach an inflection point. As shown in Fig. 10(c), the slopes of curves decrease gradually before the curves reach an inflection point. It can be discovered that the ionic liquid can be accelerated to infiltrate the emitter by decreasing β. Comparing Figs. 10(a1), 10(b1), and 10(c1) with Figs. 10(a2), 10(b2), and 10(c2) whose infiltration curves have the same θ, it is found that α has minimal effect on the emitter infiltrating velocity. There is an obvious contrast among Figs. 10(a)–10(c) that the influence of θ on the emitter infiltrating velocity and infiltrating response time t_{min} has been weakened gradually with the liquid volume growth caused by increasing β. Observing Fig. 10(a), β = −30° contained fewer liquid reserves; the emitter infiltrating velocity and infiltrating response time t_{min} are still sensitive to the change in θ. It is reflected in the increase in infiltrating response time t_{min} and the decrease in infiltrating velocity with the increasing θ. According to the infiltration law about θ in Sec. III B 2, there exists an optimal value of θ, which makes the position of P_{max} the highest. The optimal values of θ in Figs. 10(a1), 10(a2), 10(b1), 10(b2), 10(c1), and 10(c2) are 35°, 15°, 20°, 20°, 25°, and 35°, respectively, and all of the values distribute in the range of 15°–35°. Besides, the position of P_{max} can also be elevated by increasing α.

The infiltration relaxation only exists under a unique condition that the α value is small enough and becomes more and more obvious with decreasing β. Furthermore, it is found that the smaller the θ is, the more obvious the infiltration relaxation is in the event of constant β. There will be two circumstances when the position of the leading edge of the liquid climbing on the needle side reaches P_{max}. One is that the position of P_{max} is fixed, and the end of the infiltration curve becomes a horizontal straight line. It indicates that the absolute infiltrating velocity is 0, as shown in zone II. The other is the periodic infiltration oscillation at point P_{max}, and the end of the infiltration curve is manifested as a periodic fluctuation. It indicates that the average infiltrating velocity is 0, as shown in zone III. The occurrence of periodic infiltration oscillation is merely related to the type of Delaunay surface to which the meniscus belongs. The results demonstrate that the periodic infiltration oscillation will not occur on the unduloid meniscus definitely, but it may occur on the nodoid meniscus. The oscillation frequency and the oscillation amplitude are two important criteria to pass judgment on the stability of the meniscus. It deserves to be mentioned that zone II can be considered a special situation that the oscillation amplitude of zone III is 0. Smaller oscillation frequency and oscillation amplitude are conducive to the stability of the meniscus and the thrust consistency of the ILET. As shown in Fig. 10(c1) (α = 5°, β = 30°, α + β ≤ 90°), all of the menisci corresponding to different θ

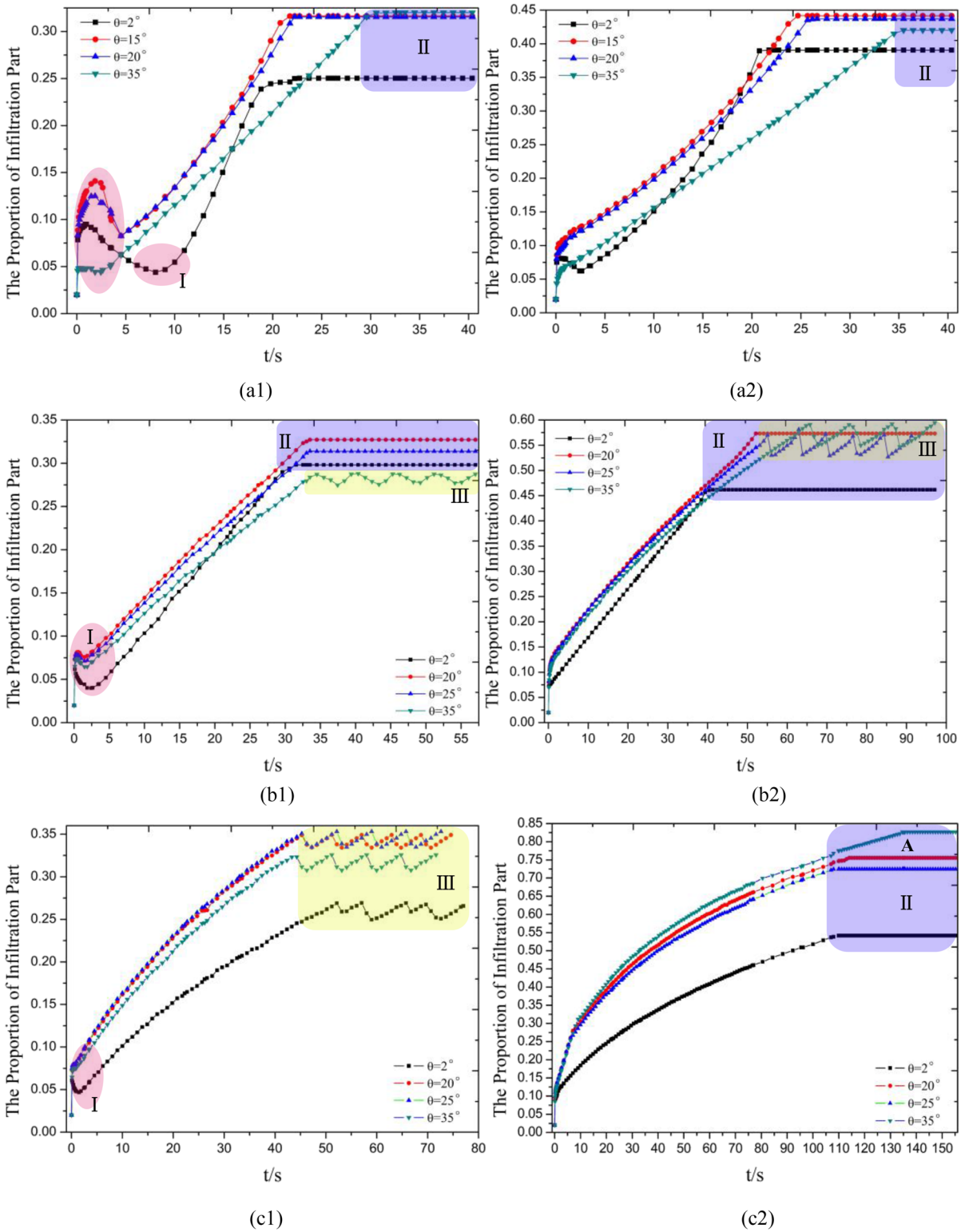

FIG. 10. L = 3 mm, d = 1 mm, γ = 1°, the effect of θ and α on dynamic infiltration. (a) β = −30°; (b) β = 0°; (c) β = 30°. (a1), (b1), and (c1) α = 5°; (a2), (b2), and (c2) α = 85°.

are nodoids in which periodic infiltration oscillation occurs without exception. The oscillation frequency will increase and the oscillation amplitude will decrease when θ rises. In particular, the infiltration curve of θ = 2° has double oscillation amplitudes. As shown in Fig. 10(c2) (α = 85°, β = 30°, α + β > 90°), all of the menisci corresponding to different θ are unduloids in which periodic infiltration oscillation does not occur. Periodic infiltration oscillation is a kind of strong nonlinearity that appears on the free surface of two-phase flow caused by the external force and boundary. In summary, the oscillation frequency and the oscillation amplitude are closely related to the variables L, d, θ, β, and α as well as the liquid properties.

3. Needle height L

As shown in Fig. 11, when θ = 22.5°mm, d = 1 mm, and γ = 1°, the effects of variables α and L on the emitter infiltrating velocity are investigated. Similarly, to research the infiltrating pattern of the nodoid and unduloid under the influence of variables α and L, it is essential to consider the emitter model that satisfies the requirement of α + β ≤ 90° or α + β > 90°; thus, two kinds of contact angles, α = 5° and α = 85°, should be set. Figure 11 (a) β = −30°, (b) β = −22.5°, (c) β = 0°, and (d) β = 30° are appropriate. Habitually, in Fig. 11(b), β = −22.5° is a distinct case that discusses the emitter model such that the needle (BC edge) is parallel to the capillary (E_iD edge).

As shown in Fig. 11, in Fig. 11(a), the emitter infiltrating velocity corresponding to different L increases slowly. In Figs. 11(b) and 11(c1), the emitter infiltrating velocity corresponding to different L remains constant. In Figs. 11(c2) and 11(d), the emitter infiltrating velocity corresponding to different L decreases gradually. It can be concluded from the above clues that reducing β is a feasible technique to accelerate the infiltrating velocity. Remarkably, the infiltration curves of the six figures have the same change rule that the emitter infiltrating velocity increases with decreasing L. There is a flagrant contrast between Figs. 11(a1), 11(b1), 11(c1), and 11(d1) and Figs. 11(a2), 11(b2), 11(c2), and 11(d2) with the same L that α almost has no effect on the emitter infiltrating velocity as usual. In addition, L has no effect on the emitter infiltrating response time t_{min}. The position of P_{max} can be elevated by decreasing L. That is to say, the proportion of infiltration part has been increased. This conclusion is consistent with the infiltration law obtained in Sec. III B 3.

As shown in Figs. 11(a1), 11(b1), 11(c1), and 11(d1) (α = 5°), the infiltration relaxation only occurs when α is small enough, and the phenomenon becomes more obvious with the decreasing β. Furthermore, it is discovered that the smaller the L is, the more obvious the infiltration relaxation is when β is constant. As shown in Fig. 11(d1) (α = 5°, β = 30°, α + β ≤ 90°), all of the menisci corresponding to different L are nodoids in which periodic infiltration oscillation occurs without exception. The oscillation frequency will decrease and the oscillation amplitude will decrease when L rises. As shown in Fig. 11(d2) (α = 85°, β = 30°, α + β > 90°), all of the menisci corresponding to different L are unduloids in which periodic infiltration oscillation does not occur.

4. Distance from needle to capillary d_i

As shown in Fig. 12, when θ = 22.5°mm, L = 3 mm, and γ = 1°, the effects of variables α and d on the emitter infiltrating velocity are investigated. For the same reason, to research the infiltrating pattern of the nodoid and unduloid under the influence of variables α and d, it is appropriate to consider the emitter model that satisfies the requirement of α + β ≤ 90° or α + β > 90°; thus, two contact angles Figs. 12(a1), 12(b1), 12(c1), and 12(d1) α = 5° and Figs. 12(a2), 12(b2), 12(c2), and 12(d2) α = 85° should be set. Figure 12 (a) β = −30°, (b) β = −22.5°, (c) β = 0° and (d) β = 30°. Habitually, in Fig. 12(b), β = −22.5° is a distinct case that discusses the emitter model such that the needle (BC edge) is parallel to the capillary (E_iD edge).

According to Sec. III B 4, the variable d has a strong nonlinear correlation with the emitter infiltration, unlike variables θ and L that show a roughly similar law of emitter infiltrating velocity corresponding to different β. Therefore, the law of emitter infiltrating velocity with regard to the variable d should be analyzed on the basis of specific α and β. The effect of d on P_{max} should be adhered to the law summarized in Sec. III B 4. The following is the effect on the emitter infiltrating velocity. As shown in Fig. 12(a) (β = −30°), the emitter infiltrating velocity increases slowly corresponding to different d. The emitter infiltrating velocity increases with the decreasing d. As shown in Fig. 12(b) (β = −22.5°), the emitter infiltrating velocity remains constant corresponding to different d. The emitter infiltrating velocity increases with the decreasing d. As shown in Fig. 12(c) (β = 0°) and Fig. 12(d) (β = 30°), the emitter infiltrating velocity decreases slowly corresponding to different d. The emitter infiltrating velocity decreases with the decreasing d. In this article, it can be concluded from the above clues once again that reducing β is a feasible technique to accelerate the infiltrating velocity. Comparing the infiltration curves that have the same d in Fig. 12, α has no effect on the infiltrating velocity as ever.

As shown in Figs. 12(a1), 12(b1), 12(c1), and 12(d1) (α = 5°) and Figs. 12(a2) and 12(b2) (α = 85°), the infiltration relaxation becomes more obvious with the decreasing β. Furthermore, it is found that the larger the d is, the more obvious the infiltration relaxation is when β is fixed. It can be illustrated from Sec. III B 4 that excessive d will lead to capillary failure. No matter how the α changes, it will not affect the emitter infiltration. The variable d directly determines the liquid reserves of the emitter. Hence, the more the liquid is reserved, the larger the residual acceleration of the liquid is, and the more the possibilities that infiltration relaxation will occur. This explains why the larger α in Figs. 12(a2) and 12(b2) (α = 85°, d = 4 mm) also causes the infiltration relaxation, which may be caused by the interaction of larger d and smaller β. When β is increased to 0° and 30°, respectively, the infiltration relaxation absolutely disappears in Figs. 12(c2) and 12(d2) (α = 85°, d = 4 mm). Observing Figs. 12(a1), 12(b1), and 12(c1) (α = 5°, d = 4 mm), the infiltration relaxation is so violent that it engulfs the climbing process of the ionic liquid with uniform velocity or slow deceleration after the infiltration relaxation and directly enters the stage of periodic infiltrating oscillation. As shown in Fig. 12(d1) (α = 5°, β = 30°, α + β ≤ 90°), all of the menisci corresponding to different d are nodoids, but only menisci with d = 1 mm and d = 4 mm cause periodic infiltration oscillation. The oscillation frequency and the oscillation amplitude will decrease when d rises. As shown in Fig. 12(d2) (α = 85°, β = 30°, α + β > 90°), all of the menisci corresponding to different d are unduloids in which periodic infiltration oscillation does not occur.

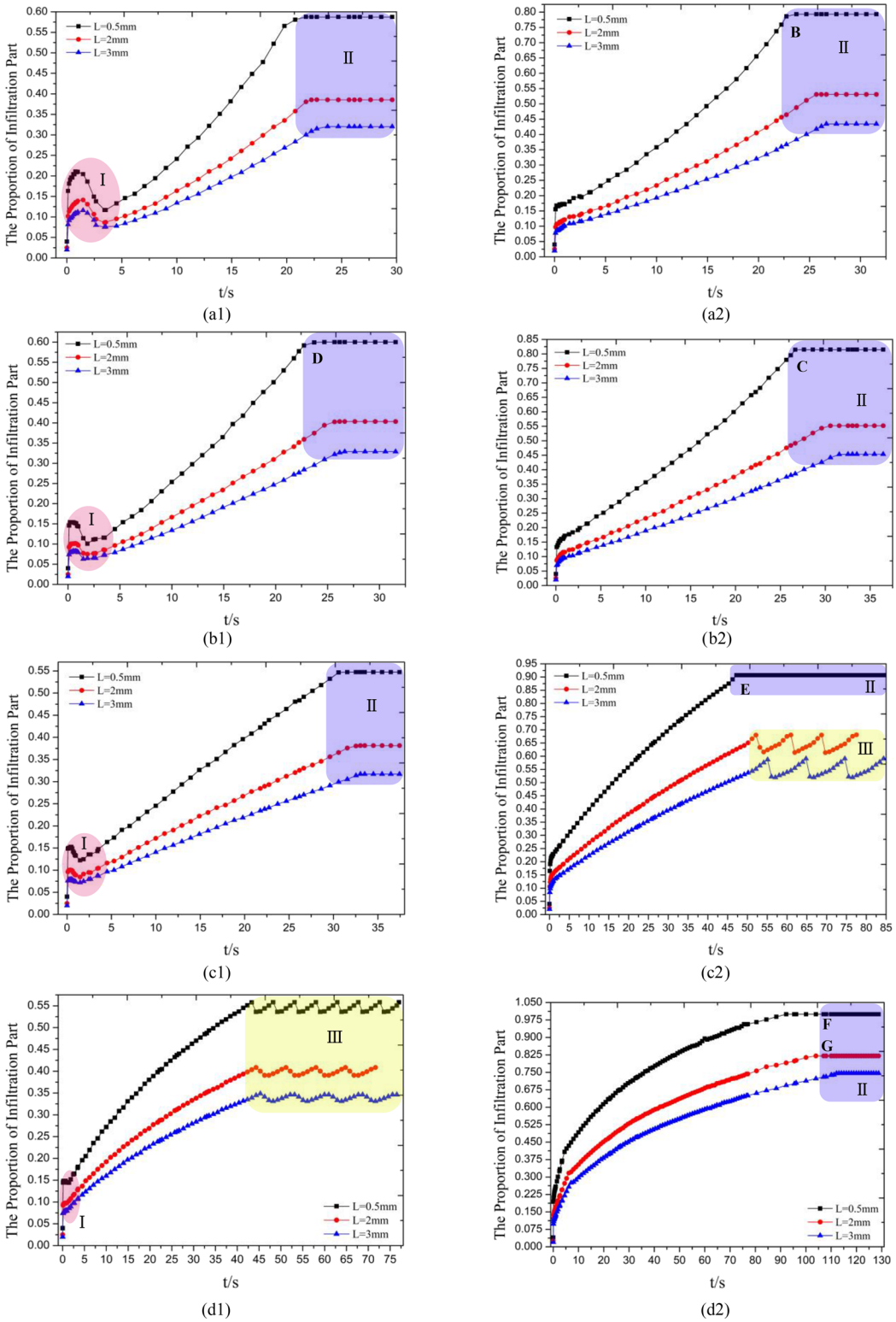

FIG. 11. θ = 22.5°, d = 1 mm, γ = 1°, the effect of L and α on dynamic infiltration. (a) β = −30°; (b) β = −22.5°; (c) β = 0°; (d) β = 30°. (a1), (b1), (c1), and (d1) α = 5°; (a2), (b2), (c2), and (d2) α = 85°.

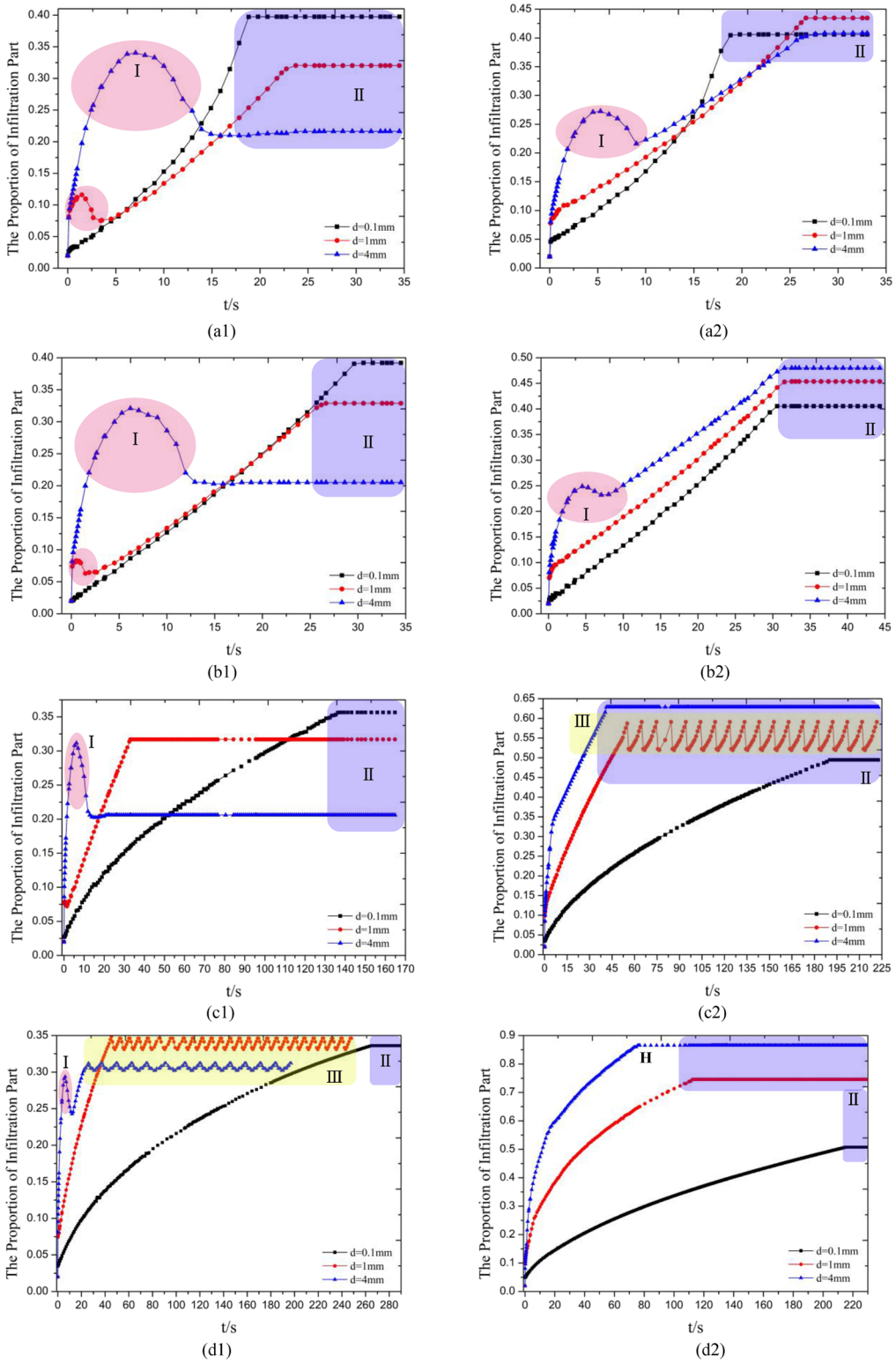

FIG. 12. θ = 22.5°, L = 3 mm, γ = 1°, the effect of d and α on dynamic infiltration. (a) β = −30°; (b) β = −22.5°; (c) β = 0°; (d) β = 30°. (a1), (b1), (c1), and (d1) α = 5°; (a2), (b2), (c2), and (d2) α = 85°.

Through the research of liquid supply condition, it is corroborated that variables L, d, and β have significant effects on the emitter infiltrating velocity. The variable θ has a weaker effect on the emitter infiltrating velocity under the premise that β is small enough. For comprehensive consideration, the variable α has no effect on the emitter infiltrating velocity.

IV. DISCUSSION

To seek out satisfied emitter infiltration of the ionic liquid electrospray thruster, the value of θ is generally deliberated between 15° and 35°. However, taking into account the low initial emission voltage and high specific impulse pure ion emission mode, θ generally does not exceed 15°. Considering the molding process and mechanical properties of the material, L and d are generally selected within 3 mm. Materials are preferred to be chosen that have the ability to provide satisfactory infiltration with ionic liquids for emitters, usually $\gamma \le 5°$. According to the infiltration law obtained in Sec. III B, the variables L, d, θ, γ, α, and β jointly affect the configuration and the infiltration of the meniscus, but only α and β are related to the classification of the Delaunay surfaces to which the meniscus belongs. Owing to the contact angle α between the ionic liquid and the capillary generally within 90° in the experiment, only $\alpha \le 85°$, $\alpha + \beta \le 90°$, and $\alpha + \beta > 90°$ are discussed in Sec. III B. However, because it is far enough from sufficient to verify the two inferences in Sec. III A, it is meaningful to discuss the other two classifications that are $\alpha > 90°$, $\beta < 0°$, $\alpha + \beta = 90°$, and $\alpha + \beta > 90°$. In order to have an intuitive comparison with Sec. III B, this paper still takes L, d, θ, and β as variables. 36 emitter models meeting the condition of $\alpha + \beta \ge 90°$ are selected randomly, which are classified by the fitting meniscus and the Delaunay surface. The fitting results are shown in Fig. 13.

According to Sec. III B and Fig. 13, the meniscus satisfying $\alpha + \beta \le 90°$ must be a nodoid definitely, and result 2 in Sec. III A is a sufficient condition. The meniscus satisfying $\alpha + \beta > 90°$ may be either an unduloid or a nodoid, and result 1 in Sec. III A is a necessary condition.

In Sec. III C, point A in Fig. 10(c2), point B in Fig. 11(a2), point C in Fig. 11(b2), point D in Fig. 11(b1), point E in Fig. 11(c2), point F and point G in Fig. 11(d2), and point H in Fig. 12(d2) are selected. These points represent the models that the proportion of infiltration part is greater than 0.6 when $\alpha = 5°$ and 0.8 when $\alpha = 85°$, respectively. There is an extremely small fitting deviation that the infiltration surface reaching the position P_{max} is used to fit the Delaunay surface, which indicates that the infiltration surface is close to the quasi-static state. So, it is reasonable to set the liquid feeding speed of 0.01 mm/s. As shown in Figs. 14(a)–14(c), 14(e), 14(g), 14(h), the larger proportion of infiltration part is achieved when $\alpha = 85°$. It is also signified that the materials that have larger contact angle between capillary and ionic liquids should be selected in order to increase the proportion of infiltration part. At the same time, larger α can effectively avoid the occurrence of infiltration relaxation. As shown in Fig. 14(f), too short L will result in an unduloid type meniscus wrapping the emitter. Meanwhile, the charged droplet emission mode is very likely to be triggered if the emission voltage is applied to the emitter. In this mode, the specific impulse loss is serious. In addition, the most serious problem may be the failure of thruster caused by short circuit between the emitter and the extractor. Therefore, in order to optimize the structure of the needle-capillary emitter, it is significant to increase the proportion of infiltration part and reduce the cross-sectional area of the liquid (the blue part in Fig. 14) on the premise of avoiding the emitter being wrapped by the ionic liquid, as shown in Fig. 14(a).

Based on the above discussion, to make the emitter get better infiltration, we should construct the emitter model that possesses the unduloid type meniscus as far as possible. The unduloid type meniscus can make more ionic liquids tend to flow along the needle side, which is conducive to emitter infiltration. In other words, the leading edge of the liquid climbing on the needle side (edge BC) is higher than that on the capillary side (edge E_iD). In addition, the emitter infiltrating velocity with the unduloid type meniscus is faster than that with the nodoid type meniscus. What is more noteworthy is that there will be no periodic infiltration oscillation if the emitter has an unduloid type meniscus. Consequently, the stability of the infiltration surface is ensured. Besides, thrust stability and consistency are improved.

If the unduloid ($a = 2.1$, $b = 1$) type meniscus described by the red dotted line is constructed in Fig. 14(a) and has the appreciable infiltration and infiltrating velocity, there must exist a corresponding infiltration surface of the emitter model shown as the blue part in Fig. 14(a). Therefore, the emitter structure size that meets the requirement of infiltration is calculated (L = 3 mm, d = 1 mm, $\theta = 35°$, $\gamma = 1°$, $\alpha = 85°$, $\beta = 30°$) through the inversion method. By analogy, the emitter structure that meets the requirements of infiltration can be determined by setting the emitter infiltration as the design constraint. Furthermore, the emitter structure with low thrust noise, reliable thrust consistency, and stability is selected as a unit of the emitter array.

Figure 15 describes the infiltrating process of the emitter model corresponding to point A in Fig. 10(c2). Because the liquid feeding speed is small enough, the infiltration surface is close to the quasi-static state and belongs to the unduloid type meniscus at all times. Consequently, the infiltrating process is called the unduloid type infiltration. In order to satisfy the condition of $\alpha + \beta > 90°$, the α of unduloid type infiltration generally is so large that the infiltration relaxation and periodic infiltration oscillation will not occur. Besides, it is guaranteed that the position of P_{max} is higher and the liquid reserves of the emitter are fewer.

Figure 16 describes the process of an unduloid type meniscus wrapping the emitter corresponding to point F in Fig. 11(d2). It also belongs to the unduloid type infiltration. In particular, the emitter is wrapped by the ionic liquid at $t_{min} = 88.298$ s because L is too short. At this moment, the needle fails and the ILET only relies on the capillary to complete the emission. The specific impulse loss is serious when the thruster enters the pure charged droplet emission mode. The excessive liquid reserves are very likely to cause the short circuit between the emitter and the extractor. Thus, the L should be shortened as much as possible on the premise that the emitter is not wrapped by ionic liquids.

Figure 17 describes the infiltrating process of the emitter model corresponding to point D in Fig. 11(b1). The residual acceleration decreases to 0 at t = 1.862 s. Because the liquid feeding speed is small

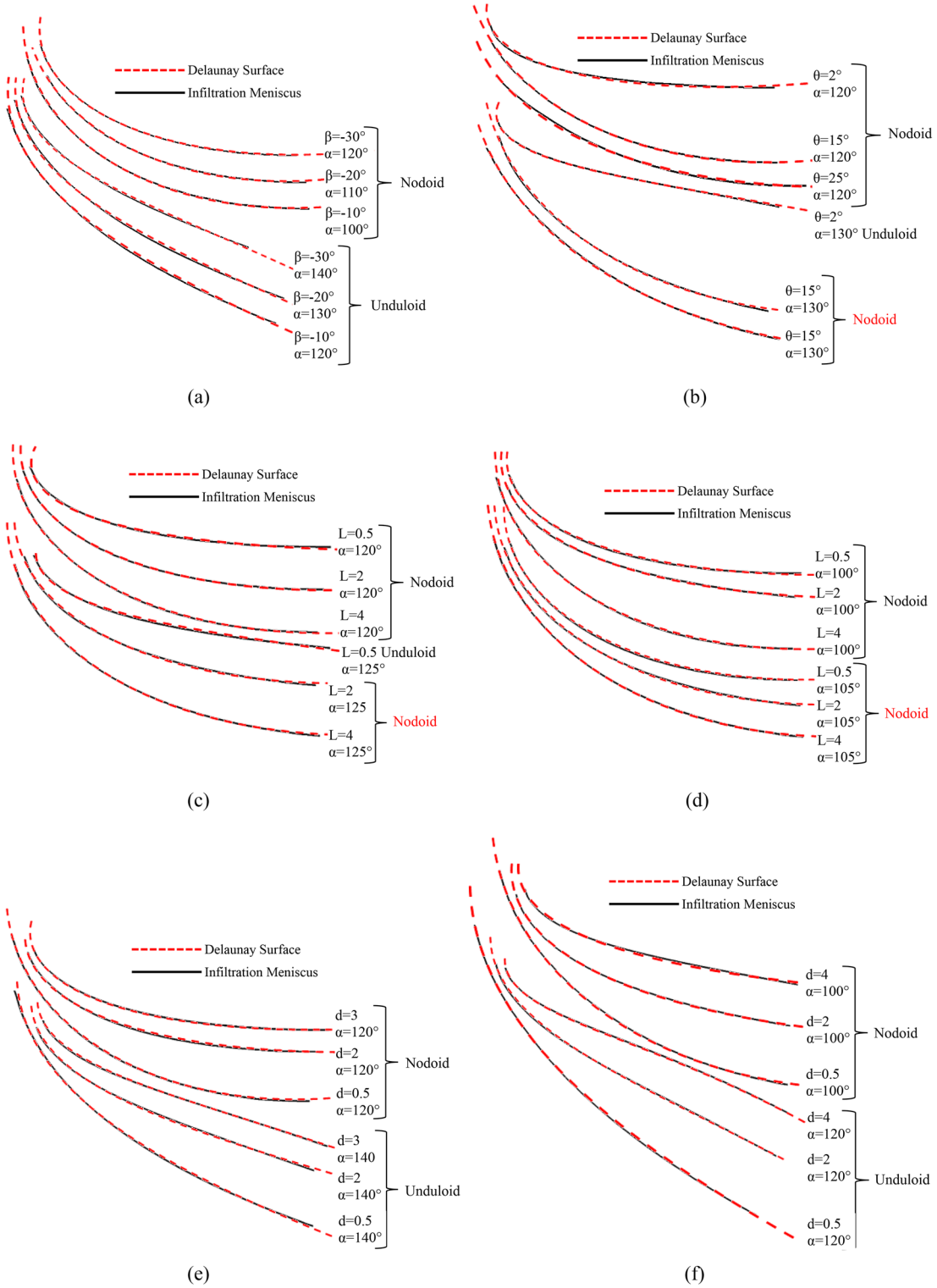

FIG. 13. $\gamma = 1°$, $\alpha + \beta \geq 90°$, the Delaunay surface and infiltration meniscus fit. (a) $\theta = 10°$, $L = 3$ mm, $d = 1$ mm, the effect of β on static infiltration. (b) $\beta = -30°$, $L = 3$ mm, $d = 1$ mm, the effect of θ on static infiltration. (c) and (d) $\theta = 10°$, $d = 1$ mm, $\beta = -30°$, and $\beta = -10°$, the effect of L on static infiltration. (e) and (f) $\theta = 10°$, $L = 3$ mm, $\beta = -30°$, and $\beta = -10°$, the effect of d on static infiltration.

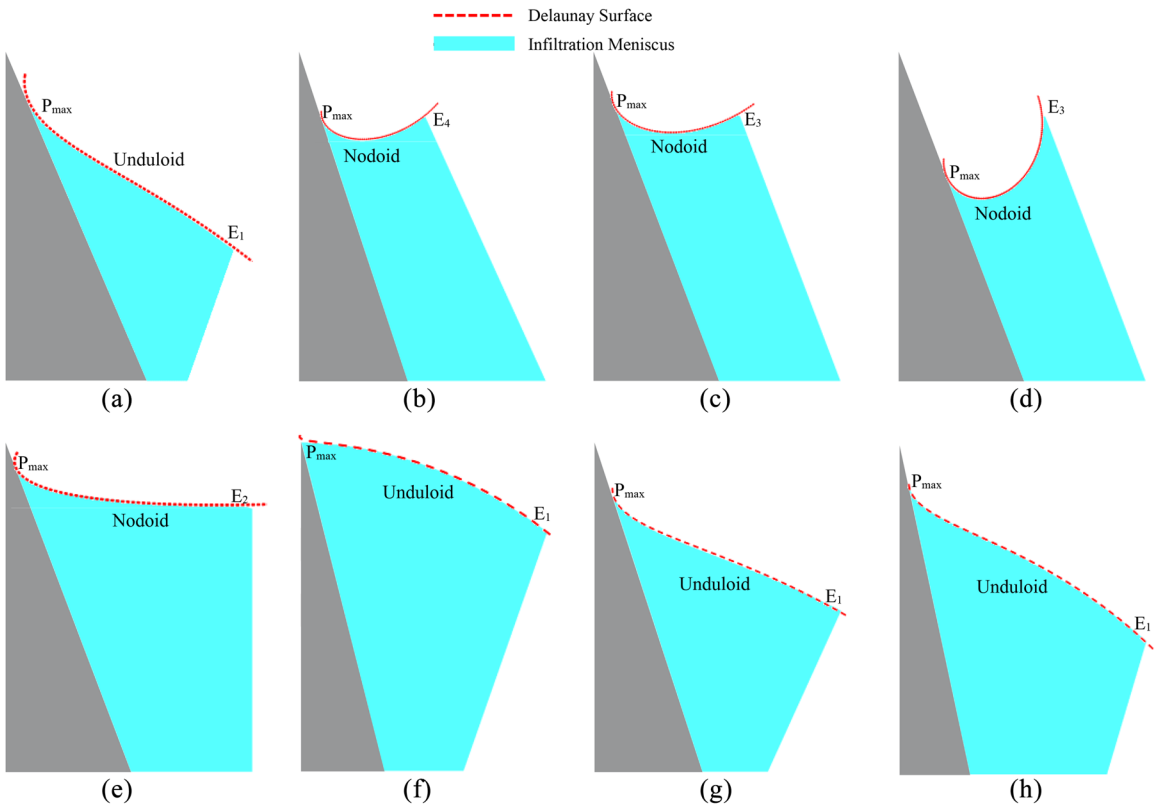

FIG. 14. Meniscus morphology of reaching the maximum infiltration percentage. (d) represents the model that the proportion of infiltration part is greater than 0.6 when $\alpha = 5°$. (f) represents the model with too short L results in an unduloid type meniscus wrapping the emitter. (a)–(c), (e), (g), and (h) represent the models that the proportion of infiltration part is greater than 0.8 when $\alpha = 85°$.

enough, the infiltration surface is close to the quasi-static state and belongs to the nodoid type meniscus at $t > 1.862$ s when the residual acceleration decreases to 0. Accordingly, the infiltrating process is called the nodoid type infiltration. In order to satisfy the condition of $\alpha + \beta \leq 90°$, the α is small enough to induce the infiltration relaxation occurring in the time range from $t = 0.098$ s to $t = 1.862$ s. The datum line passes through the leading edge of the liquid climbing on the needle side at $t = 0.392$ s. The tendency can be clearly observed that the proportion of infiltration part increases first and then decreases. More crucially, by reviewing all emitter models belonging to nodoid type infiltration in Sec. III C, it is found that the periodic infiltration oscillation will not occur definitely when $\beta < 0°$. On the contrary,

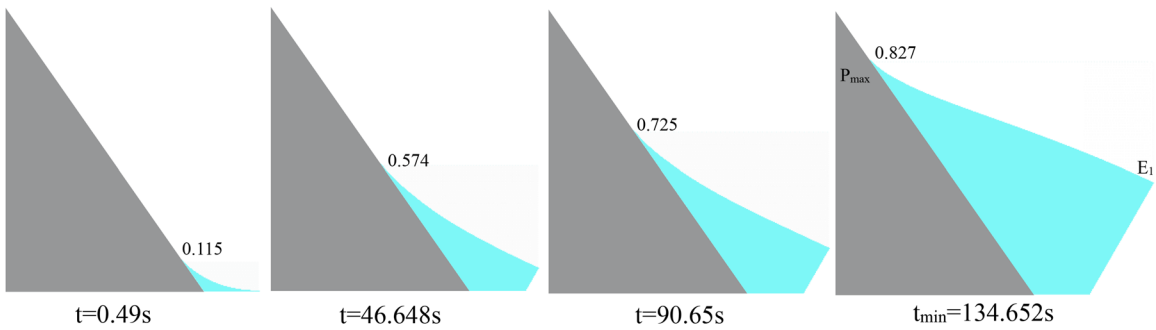

FIG. 15. $\theta = 35°$, $\beta = 30°$, L = 3 mm, d = 1 mm, $\alpha = 85°$, $\gamma = 1°$, the process of an unduloid infiltrating emitter.

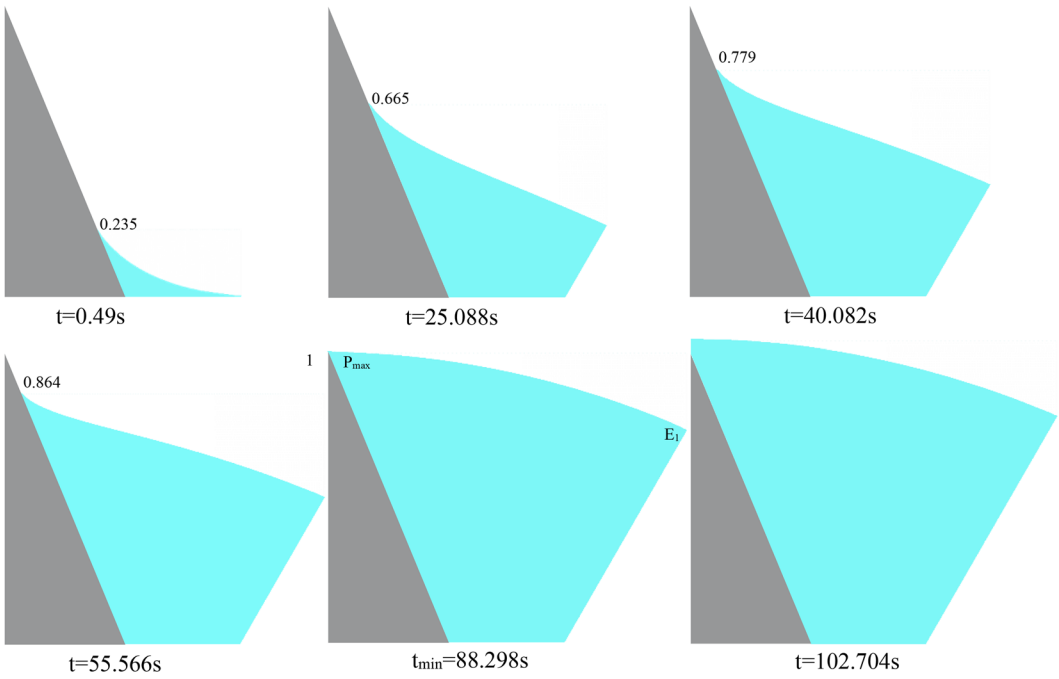

FIG. 16. θ = 22.5°, β = 30°, L = 0.5 mm, d = 1 mm, α = 85°, γ = 1°, the process of an unduloid type meniscus wrapping the emitter.

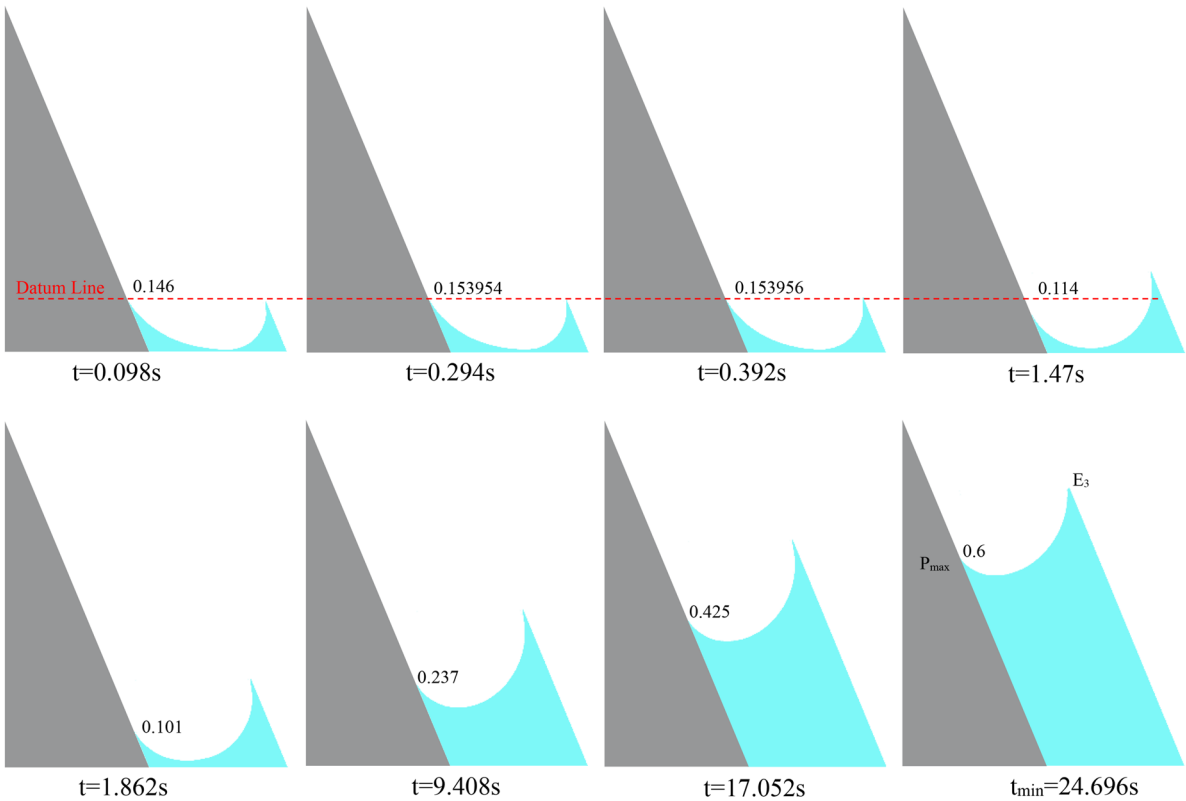

FIG. 17. θ = 22.5°, β = −22.5°, L = 0.5 mm, d = 1 mm, α = 5°, γ = 1°, the process of the nodoid infiltrating emitter.

the periodic infiltration oscillation may occur or may not occur when $\beta \geq 0^\circ$.

V. CONCLUSION

As an important part of electric propulsion technology, the ionic liquid electrospray thruster has great application potential in satellite formation flight, attitude control, orbit maintenance, and disturbance cancellation. Different emitter structures show their own unique emission performance. In this paper, a new type of emitter structure is proposed to solve the problems of unstable thrust, high noise, and poor consistency caused by no infiltration, non-uniform infiltration, or discontinuous infiltration, which the traditional external infiltration type emitter cannot avoid. The law of emitter infiltration and emitter infiltrating velocity is concluded by studying the conditions of no liquid supply and liquid supply separately. The infiltration phenomena caused by variables L, d, β, θ, and α are discussed in detail. From the perspective of fitting results and infiltration effect, the numerical simulation method used in this paper has acceptable minimum error. It also supports that the technical path is feasible to improve the emitter infiltration effect by optimizing the variables L, d, β, θ, and α.

Under the condition of no liquid supply, the infiltration curve trend rises in a parabola with the increasing inclination angle of the capillary β. It can be found from Fig. 2(a1) that the revenue growth rate of emitter infiltration is significantly accelerated when $\beta \geq 20^\circ$. The capillary (edge E_iD) has the functions of liquid storage, transportation, and management. If β is too large, the liquid reserves of the emitter will be too much, which will result in low precision of liquid supply, weak liquid level repositioning ability, and poor liquid anti-sway ability, and even the emitter array will be polluted. It is impossible to obtain greater infiltration revenue by continuously increasing β. The good news is that increasing α to increase wettability is another practical approach. On the premise that the β is as large as possible, the unduloid type infiltration meeting the requirement of $\alpha + \beta > 90^\circ$ should be constructed, so as to obtain the largest proportion of infiltration part and the fewest liquid reserves. Furthermore, the infiltration curve trend declines in a parabola approximatively with the increasing height of the needle exposed to the capillary L. Therefore, it should be ensured that the smaller L should be selected as far as possible on the premise that the emitter is not wrapped by the ionic liquid. When the shortest distance from the needle to the capillary $d \leq 3$ mm, the variable d has a greater impact on the emitter infiltration. Within this range, it ensures fewer liquid reserves and highlights the functions of the capillary in liquid storage, transportation, and management. Though there exists an optimal θ that makes the emitter infiltration best, the optimal value of θ should be explored by drawing the infiltration curve about the variable θ after determining the variables α, β, L, and d.

Under the condition of liquid supply, the emitter infiltrating velocity increases with the decreasing inclination angle of the capillary β. Besides, the emitter infiltrating velocity increases with the decreasing height of the needle exposed to the capillary L. In particular, the influence of the shortest distance from the needle to the capillary d on the emitter infiltrating velocity needs to be analyzed based on specific α and β. On the contrary, θ will affect the emitter infiltrating velocity when β is small enough. α has no effect on the emitter infiltrating velocity.

Infiltration and infiltrating velocity are the most urgent problems that need to be conquered for the external infiltration type ionic liquid electrospray thruster. This article has summarized abundant achievements that are related to the law of needle-capillary emitter infiltration and infiltrating velocity. This research provides reasonable design constraints for the optimization of the needle-capillary ILET. Compared with Secs. III B and III C, it is found that the optimal infiltration and the optimal infiltrating velocity cannot be satisfied at the same time. Consequently, it is significant to select an appropriate balance point to optimize the emitter according to different space missions. The actual infiltration effect needs to be tested by the emission experiment. Because ionic liquids have strong conductivity as propellants, it is ineluctable to study the emitter infiltration under the condition of considering electric field. The concept of electrowetting adds a new connotation to the external infiltration type ILET.

ACKNOWLEDGMENTS

This work was supported by the Strategic Priority Research Program of the Chinese Academy of Sciences (No. XDB23030300) and the National Natural Science Foundation of China (Grant Nos. 12032020 and 12072354).

DATA AVAILABILITY

The data that support the findings of this study are available from the corresponding author upon reasonable request.

REFERENCES

[1] C. Williams, S. Delpozzo, and B. Doncaster, *Nano/Microsatellite Market Forecast*, 9th ed. (Space Works Enterprises, Inc., 2019).
[2] J. Ziemer, M. Gamero-Castaño, V. Hruby *et al.*, "Colloid micro-Newton thruster development for the ST7-DRS and LISA missions," in AIAA/ASME/SAE/ASEE Joint Propulsion Conference and Exhibit, 2005.
[3] N. R. Demmons, D. Courtney, N. Alvarez *et al.*, "Component-level development and testing of a colloid micro-thruster (CMT) system for the LISA mission," in AIAA Propulsion and Energy 2019 Forum, 2019.
[4] M. Gamero-Castaño, R. E. Wirz *et al.*, "LISA colloid microthruster technology development plan and progress," in International Electric Propulsion Conference, 2019.
[5] J. Ziemer, C. Marrese-Reading, C. Dunn *et al.*, "Colloid microthruster flight performance results from space technology 7 disturbance reduction system," in 35th International Electric Propulsion Conference, Atlanta, USA, 2017.
[6] B. L. P. Gassend, "A fully microfabricated two-dimensional electrospray array with applications to space propulsion," in Ph.D. dissertation (Massachusetts Institute of Technology, Cambridge, 2007).
[7] J. Zwahlen, V. Hruby, C. Campbell *et al.*, "Flow control micro-valve for the ST7-DRS colloid thruster," in 44th AIAA/ASME/SAE/ASEE Joint Propulsion Conference and Exhibit, Hartford, CT, USA, 2008.
[8] R. S. Legge and P. C. Lozano, "Electrospray propulsion based on emitters microfabricated in porous metals," J. Propul. Power **27**(2), 485–495 (2011).
[9] D. G. Courtney, H. Q. Li, and P. Lozano, "Emission measurements from planar arrays of porous ionic liquid ion sources," J. Phys. D: Appl. Phys. **45**(48), 485203 (2012).
[10] C. Guerra-Garcia, D. Krejci, and P. Lozano, "Spatial uniformity of the current emitted by an array of passively fed electrospray porous emitters," J. Phys. D: Appl. Phys. **49**(11), 115503 (2016).

[11]D. Krejci and P. Lozano, "Scalable ionic liquid electrospray thrusters for nanosatellites," in 39th Annual Guidance and Control Conference, Breckenridge, CO, 2016.
[12]P. L. Wright, H. Huh, N. M. Uchizono *et al.*, "A novel variable mode emitter for electrospray thrusters," in International Electric Propulsion Conference, 2019.
[13]J. Eells, "The surfaces of Delaunay," Math. Intell. **9**(1), 53–57 (1987).
[14]H. N. G. Nguyen, O. Millet, and G. Gagneux, "On the capillary bridge between spherical particles of unequal size: Analytical and experimental approaches," Continuum Mech. Thermodyn. **31**, 225 (2018).
[15]G. Lian, C. Thornton, and M. J. Adams, "A theoretical study of the liquid bridge forces between two rigid spherical bodies," J. Colloid Interface Sci. **161**(1), 138–147 (1993).
[16]B. Athukorallage, T. Paragoda, and M. Toda, "Roulettes of conics, Delaunay surfaces and applications," Surv. Math. Math. Sci. **4**(1), 1–20 (2014).